



Retrieval of water  
vapour around PMCs  
from Odin-SMR

O. M. Christensen et al.

This discussion paper is/has been under review for the journal Atmospheric Measurement Techniques (AMT). Please refer to the corresponding final paper in AMT if available.

# Tomographic retrieval of water vapour and temperature around polar mesospheric clouds using Odin-SMR

O. M. Christensen<sup>1</sup>, P. Eriksson<sup>1</sup>, J. Urban<sup>1,†</sup>, D. Murtagh<sup>1</sup>, K. Hultgren<sup>2</sup>, and J. Gumbel<sup>2</sup>

<sup>1</sup>Department of Earth and Space Sciences, Chalmers University of Technology, Gothenburg, Sweden

<sup>2</sup>Department of Meteorology, Stockholm University, Stockholm, Sweden

<sup>†</sup>deceased, 14 August 2014

Received: 8 October 2014 – Accepted: 6 November 2014 – Published: 28 November 2014

Correspondence to: O. M. Christensen (ole.m.christensen@chalmers.se)

Published by Copernicus Publications on behalf of the European Geosciences Union.

Title Page

Abstract

Introduction

Conclusions

References

Tables

Figures



Back

Close

Full Screen / Esc

Printer-friendly Version

Interactive Discussion



## Abstract

A special observation mode of the Odin satellite provides the first simultaneous measurements of water vapour, temperature and polar mesospheric cloud (PMC) brightness over a large geographical area while still resolving both horizontal and vertical structures in the clouds and background atmosphere. The observation mode has been activated during June, July and August of 2010, 2011 and 2014, and for latitudes between 50 and 82° N.

This paper focuses on the water vapour and temperature measurements carried out with Odin's sub-millimetre radiometer (SMR). The tomographic retrieval approach used provides water vapour and temperature between 75–90 km with a vertical resolution of about 2.5 km and a horizontal resolution of about 200 km. The precision of the measurements is estimated to 0.5 ppm for water vapour and 3 K for temperature. Due to limited information about the pressure at the measured altitudes, the results have large uncertainties (> 3 ppm) in the retrieved water vapour. These errors, however, influence mainly the mean atmosphere retrieved for each orbit, and variations around this mean are still reliably captured by the measurements.

SMR measurements are performed using two different mixer chains, denoted as frequency mode 19 and 13. Systematic differences between the two frontends have been noted. A first comparison with the Solar Occultation For Ice Experiment instrument (SOFIE) on-board the Aeronomy of Ice in the Mesosphere (AIM) satellite and the Fourier Transform Spectrometer of the Atmospheric Chemistry Experiment (ACE-FTS) on-board SCISAT indicates that the measurements using the frequency mode 19 have a significant low bias in both temperature (> 20 K) and water vapour (> 1 ppm), while the measurements using frequency mode 13 agree with the other instruments considering estimated errors.

PMC brightness data are provided by the OSIRIS, Odin's other sensor. Combined SMR and OSIRIS data for some example orbits are considered. For these orbits, effects of PMCs on the water vapour distribution are clearly seen. Areas depleted of water

## Retrieval of water vapour around PMCs from Odin-SMR

O. M. Christensen et al.

Title Page

Abstract

Introduction

Conclusions

References

Tables

Figures



Back

Close

Full Screen / Esc

Printer-friendly Version

Interactive Discussion



vapour are found above layers with PMC, while regions of enhanced water vapour due to ice particle sedimentation are primarily placed between and under the clouds.

## 1 Introduction

Noctilucent, or Polar mesospheric clouds (PMCs) are ice-clouds that form in the summer mesopause region at high latitudes. During the last 30 years there has been much research focused on understanding the formation and development of these clouds. In particular, the question has been raised as to how these clouds are responding to the anthropogenic release of greenhouse gases (Thomas et al., 1989), and whether or not these clouds could be used as an indicator of large scale climate change affecting the mesopause region (von Zahn, 2003; Thomas et al., 2003).

To accurately understand possible changes and predict the future of PMCs, we need to understand the micro-physical properties of the clouds and the conditions under which they form (Rapp and Thomas, 2006; Lübken et al., 2007). The formation of PMCs is governed by the amount of supersaturation of the local atmosphere, thus good measurements of temperature and water vapour in the mesopause region are needed to accurately assess models and to identify the processes involved in the creation and sublimation of PMCs (Russell et al., 2009).

Water vapour and temperature in the vicinity of PMCs have been measured in several studies using ground-, satellite- as well as rocket based instruments (e.g. Lübken et al., 1999; Seele and Hartogh, 1999; Sheese et al., 2011). However, for accurate comparisons to models, both water vapour and temperature should ideally be measured simultaneously. Such measurements are less common, and have to date mainly been provided by solar occulting instruments such as HALOE (McHugh et al., 2003), ACE-FTS (Zasetsky et al., 2009) and AIM-SOFIE (Hervig et al., 2009). These measurements have been used in several studies (e.g. Rong et al., 2012; Zasetsky et al., 2009) to investigate the relationship between the background atmosphere and PMCs.

### Retrieval of water vapour around PMCs from Odin-SMR

O. M. Christensen et al.

Title Page

Abstract

Introduction

Conclusions

References

Tables

Figures



Back

Close

Full Screen / Esc

Printer-friendly Version

Interactive Discussion



## Retrieval of water vapour around PMCs from Odin-SMR

O. M. Christensen et al.

Title Page

Abstract

Introduction

Conclusions

References

Tables

Figures



Back

Close

Full Screen / Esc

Printer-friendly Version

Interactive Discussion



Unfortunately, solar occulting instruments have a limitation when it comes to the horizontal sampling of the atmosphere. Since only one profile is generated in each hemisphere per orbit, latitudinal variations of the atmosphere can only be investigated on a seasonal basis using these instruments. Emission limb sounders can, unlike solar occulting instruments, provide global maps of water vapour and temperature across the entire PMC region within a day. And, unlike infrared emission sounders (López-Puertas et al., 2009; Feofilov et al., 2009), instruments operating in the microwave region do not have to account for non-LTE emissions. Accordingly, the microwave limb sounder (MLS) on board Aura has been used to study the latitudinal variations in cloud formation (Rong et al., 2014). However, due to the limited vertical resolution of MLS at the altitudes of concern, and the fact that a second satellite instrument (AIM-CIPS) had to be used for the PMC data, only horizontal variations could be studied.

For a complete picture of the relevant processes involved in the PMC formation, high resolution and good coverage in both the vertical and horizontal directions of the background atmosphere and the PMC distribution is required. In this paper we present a set of measurements by the sub-millimetre radiometer (SMR) on board the Odin satellite, which for the first time provides high resolution water vapour and temperature measurements around PMCs with a large geographical coverage. Simultaneous measurements are performed of PMC brightness by the Optical Spectrograph and InfraRed Imager System (OSIRIS) on Odin, and as such the combined observations provide a unique dataset useful for the study of PMC formation.

SMR measures a water vapour transition at 556.9 GHz. In the normal operational mode it scans the atmosphere between 10 and 110 km, and retrieves both water vapour and temperature. This measurement mode has in been used earlier studies to investigate the water vapour distribution in the mesosphere and above (Lossow et al., 2009). However, since the normal scanning covers the entire middle atmosphere, the horizontal distance between scans can be over 1000 km (Lossow et al., 2007), which make retrievals of water vapour and temperature around PMCs with a high horizontal resolution impossible.

## Retrieval of water vapour around PMCs from Odin-SMR

O. M. Christensen et al.

Title Page

Abstract

Introduction

Conclusions

References

Tables

Figures



Back

Close

Full Screen / Esc

Printer-friendly Version

Interactive Discussion



To increase the horizontal sampling rate, a set of measurements was made in a special “tomographic” mode during June, July and August 2010, 2011 and 2014. In this mode only altitudes between 75 and 90 km are scanned, which reduces the distance between scans to 200 km, thus allowing for a much higher horizontal resolution. As an additional advantage, the increased density of measurements opens the possibility of tomographically retrieving the atmospheric fields using a 2-dimensional retrieval algorithm. Tomographic algorithms have been used by several different limb sounding instruments (Degenstein et al., 2003; Steck et al., 2005; Livesey et al., 2006; Pu $\text{u}\text{t}\text{i}\text{t}\text{e}$  et al., 2008), and they allow the retrieval method to take into account inhomogeneities along the line of sight. Thus, the sensitivity and resolution of the measurements can be improved further compared to the operational SMR retrievals.

The co-aligned measurements of PMC brightness performed by OSIRIS are described in Hultgren et al. (2013). A tomographic approach is used to retrieve both vertical and horizontal structures of the PMCs with a horizontal resolution down to 330 km and a vertical resolution of 1 km. Combined, the two instruments on board Odin can thus provide measurements of water vapour, temperature and PMC brightness with a hitherto unprecedented spacial resolution and coverage. SMR also performed similar measurements of the Southern Hemisphere during 2011, but these lack co-located OSIRIS measurements, and have a slightly different measurement geometry, and as such will not be considered in this study.

The goal of this paper is to give a detailed description of the tomographic SMR retrievals, and assess their capabilities and limitations in the retrieval of the background atmosphere around PMCs. We will first describe the instrument and the measurement procedure (Sect. 2), before moving on to the retrieval methodology (Sect. 3). The first results from the measurements are shown in Sect. 4, and the accuracy and reliability of the measurements will be discussed in Sect. 5. Finally, we compare the results to other satellite instruments and show some early results combining SMR and OSIRIS data before summarising our findings in Sect. 6.





## Retrieval of water vapour around PMCs from Odin-SMR

O. M. Christensen et al.

Title Page

Abstract

Introduction

Conclusions

References

Tables

Figures



Back

Close

Full Screen / Esc

Printer-friendly Version

Interactive Discussion



The amount of noise in each channel is determined by the noise temperature of the system, the effective channel resolution, and the integration time. For the frequency bands used in this study, SMR has a noise temperature of roughly 3000–3500 K. For the tomographic mode measurements, an integration time of 1.8 s is used. Due to the time used switching between calibration measurements and atmospheric measurements SMR is only measuring the atmosphere about only half of the total time. Taking this into account, the resulting thermal noise ( $1\sigma$ ) is in the order of 2.6 K for the measured spectra.

To relate the measured radiation to a physical brightness temperature a calibration must be performed. The SMR measurements are calibrated by switching between the cold sky (space) and the atmosphere, with a hot-load calibration performed at the end of each scan. In this study the newest version (V8) of the calibrated Odin spectra is used. This version was prepared during the autumn of 2013, and beside improving the treatment of known instrumental artefacts, it corrected an error related to the transition between orbits, which previously had made the tomographic observations unusable.

The vertical resolution of the measurements depends on the size and shape of the antenna pattern. For SMR the antenna is a 1.1 m Georgian telescope which provides a half power beam width better than  $0.035^\circ$  (Frisk et al., 2003). This results in a vertical resolution at the tangent point of  $\sim 1.6$  km. However, due to the telescope continuously scanning vertically during the integration time of 1.8 s the angular resolution is reduced to  $0.04^\circ$  ( $\sim 1.8$  km) in the tomographic mode.

### 2.3 OSIRIS

In addition to presenting the results from the SMR tomographic mode retrievals, this paper also includes some comparisons with the PMC brightness retrieved from the optical spectrograph of OSIRIS. The spectrograph is a modified Erbert–Fastie grating spectrometer with a CCD backend, and can measure light scattered from the atmosphere between 280 and 800 nm with a spectral resolution of around 1 nm. The entrance slit of

OSIRIS is aligned parallel to the horizon, and subtends a region 30 km wide and 1 km high at the tangent point.

To retrieve PMC properties from the scattered light, the measured radiation in the wavelength region of 302.8 to 305.9 nm is compared to a purely Rayleigh scattering background field calculated using the MSIS climatology. The differences between the measured and simulated spectra are then used as inputs to a tomographic retrieval scheme based on a modified version of the Multiplicative Algebraic Reconstruction Technique (MART, Degenstein et al., 2003). The retrievals return the scattering coefficient of the clouds with a 330 km horizontal resolution and 1 km vertical resolution, and an accuracy of  $4 \times 10^{-11} \text{ m}^{-1} \text{ str}^{-1}$ . For a detailed description of the observations and retrieval process the reader is referred to Hultgren et al. (2013).

### 3 Retrieval methodology

To extract atmospheric data from the SMR measurements the optimal estimation method (OEM) is applied. ARTS (Atmospheric Radiative Transfer Simulator) is used as the forward model, and the retrieval procedure is implemented using a software package accompanying ARTS. As previously mentioned, the overlapping lines-of-sight for the measurements allows for a tomographic retrieval approach. This means that a two dimensional (2-D) map of the atmospheric fields is retrieved, rather than single vertical profiles. The following section describes the forward model and retrieval procedure used in this study.

#### 3.1 Forward model

##### 3.1.1 General about ARTS

ARTS is a general purpose radiative transfer program, with a focus on supporting passive microwave sounding techniques (Buehler et al., 2005). It is publicly available software. The second version of ARTS (Eriksson et al., 2011) allows simulations for 1-D,

## Retrieval of water vapour around PMCs from Odin-SMR

O. M. Christensen et al.

Title Page

Abstract

Introduction

Conclusions

References

Tables

Figures



Back

Close

Full Screen / Esc

Printer-friendly Version

Interactive Discussion





ever, due to the large computational demands posed by the tomographic retrieval approach, an entire orbit cannot be processed simultaneously on a desktop computer (32 GB RAM) unless data reduction techniques are applied. To keep the processing scheme simple, we have chosen not to apply any such techniques, but instead split the measurements into “batches” of 12 scans ( $\sim 150$  spectra) covering  $\sim 40^\circ$  AAO (see Fig. 1a). This results in the forward model horizontal grid for each batch covering  $\pm 30^\circ$  AAO ( $\sim 4500$  km) around the centre of the batch with a resolution of  $0.25^\circ$  ( $\sim 30$  km). Outside this area 16 additional gridpoints cover the AAOs up to  $\pm 50^\circ$  AAO with a lower resolution to ensure that no errors arise from edge effects.

### 3.1.3 Frequency grid and line parameters

ARTS is a line-by-line radiative transfer simulator, and for simulation of the 556.9 GHz water vapour transition we use a monochromatic frequency grid ranging from 556.5 to 557.5 GHz. The resolution is 100 kHz around the line centre (556.925 to 556.945 GHz) decreasing further away from the line centre reaching 100 MHz at the far end of the grid. In addition to the frequencies in the signal band, some frequencies are added in the image band to accurately take into account influence of the sideband filtering. For the simulations in this study involving just a handful of transitions, absorption is best calculated for each point along the propagation paths (“on the fly” in ARTS terminology), as the option of using a pre-calculated look-up table is slower.

The line parameters for the water vapour line are taken from JPL and HITRAN2012. JPL (Pickett et al., 1998) is used for the line position (556.9359877 GHz) and the line strength ( $229.8489 \text{ Hz/m}^2$ ). HITRAN2012 (Rothman et al., 2013) is used for the pressure broadening coefficient  $\gamma_p$ . The coefficient is calculated as  $\gamma_p(p, T) = p\gamma_{\text{air}}(T/T_0)^n$ , where  $\gamma_{\text{air}} = 31\,362.45 \text{ Hz Pa}^{-1}$  is the pressure broadening parameter,  $T$  the atmospheric temperature,  $T_0 = 296 \text{ K}$  the reference temperature for the broadening parameters, and  $n = 0.75$  the exponent of the temperature dependency.

## Retrieval of water vapour around PMCs from Odin-SMR

O. M. Christensen et al.

Title Page

Abstract

Introduction

Conclusions

References

Tables

Figures



Back

Close

Full Screen / Esc

Printer-friendly Version

Interactive Discussion



### 3.1.4 Instrument

ARTS includes extensive support for incorporating instruments characteristics. Using the methodology introduced by Eriksson et al. (2002, 2006), monochromatic pencil beam spectra are combined, taking into account the response of antenna, mixer sidebands and spectrometer, to simulate final sensor brightness temperatures. For this study, the modelled antenna pattern is based on the measurements of the SMR antenna system, the single sideband filter is modelled as a flat function with a sideband suppression of 14 dB, and the spectrometer backend channel response is based on a theoretical model of the spectrometer.

## 3.2 Retrieval

### 3.2.1 General OEM

In the optimal estimation method the retrieved state vector,  $\hat{\mathbf{x}}$ , is the one minimising the a posteriori error, based on the known, or assumed, properties of the variations of the atmosphere and errors in the observation (Rodgers, 2000). Due to the non-linearity of the retrievals in this study an iterative Levenberg–Marquard method is applied. The state vector of iteration  $i + 1$  from the OEM method is then given by

$$\hat{\mathbf{x}}_{i+1} = \hat{\mathbf{x}}_i + \left[ (1 + \gamma) \mathbf{S}_a^{-1} + (\mathbf{K}_i^T \mathbf{S}_e^{-1} \mathbf{K}_i) \right]^{-1} \left[ \mathbf{K}_i^T \mathbf{S}_e^{-1} (\mathbf{y} - f(\mathbf{x}_i)) - \mathbf{S}_a^{-1} (\mathbf{x}_i - \mathbf{x}_a) \right], \quad (1)$$

where  $\mathbf{S}_a$  and  $\mathbf{S}_e$  are the covariance matrices for the apriori state vector,  $\mathbf{x}_a$ , and the thermal noise in the measurement given by  $\mathbf{y}$ .  $\mathbf{K}_i$  is the Jacobian matrix calculated using the forward model of iteration  $i$ ,  $f(\mathbf{x}_i)$ .  $\gamma$  is the Levenberg–Marquard parameter. It is adjusted after each iteration based on whether the cost function to be minimised is decreased or increased by the iteration. For the first iteration  $\mathbf{x}_1 = \mathbf{x}_a$  and  $\gamma = 500$ . For each successful iteration  $\gamma$  is divided by ten, and for each failed iteration it is doubled. Convergence is reached when the change in the retrieved state vectors between itera-

## Retrieval of water vapour around PMCs from Odin-SMR

O. M. Christensen et al.

Title Page

Abstract

Introduction

Conclusions

References

Tables

Figures

◀

▶

◀

▶

Back

Close

Full Screen / Esc

Printer-friendly Version

Interactive Discussion



tions, normalised by the apriori covariance, is less than 0.01. For most cases this is achieved after 7–10 iterations, and the final normalised costs are between 0.9–1.1.

### 3.2.2 The state vector

The state vector contains all the variables to be retrieved, and in this study the state vector consists of the amount of atmospheric water vapour relative to the apriori ( $H_2O$ ), atmospheric temperatures in Kelvin ( $T$ ) and some instrument variables. These variables are a baseline fit, a frequency shift and a fit of the pointing error. The instrumental baseline arises due to standing waves in the receiver, and to fit this, a first order polynomial is fitted to each spectrum ( $P_0, P_1$ ). The exact positioning of the LO frequency has some uncertainty. This is fitted with a single frequency fit ( $\Delta F$ ) across each batch. Finally there is an uncertainty in the pointing of the antenna, and a single pointing offset ( $\Delta\theta$ ) is retrieved across the batch.

The total state vector is given by combining all the sub vectors

$$\mathbf{x} = [H_2O, T, \Delta F, \Delta\theta, P_0, P_1]^T. \quad (2)$$

For the atmospheric fields ( $H_2O, T$ ) the elements are sorted first by altitude then by latitude and the retrieval grid covers altitudes between 316 Pa ( $\sim 40$  km) to 0.75 mPa ( $\sim 130$  km) with an altitude resolution of 1 km above 17 Pa ( $\sim 60$  km) and a resolution of 2 km below. The horizontal retrieval grid covers  $50^\circ$  AAO centred around the batch with a resolution of  $0.5^\circ$ .

### 3.2.3 Apriori values

For each state vector variable an apriori value must be given. For the atmospheric variables, these are given as two dimensional fields across the retrieval grid. For water vapour, an apriori profile constant with latitude and time was chosen. Using such a fixed apriori profile makes it easier to ensure that the structures seen in the retrieved water vapour field actually come from the measurements, rather than the apriori field.

## Retrieval of water vapour around PMCs from Odin-SMR

O. M. Christensen et al.

Title Page

Abstract

Introduction

Conclusions

References

Tables

Figures



Back

Close

Full Screen / Esc

Printer-friendly Version

Interactive Discussion



The apriori profile is based on a climatology of water vapour from the MLS instrument on board the AURA satellite. Taking the mean of the MLS water vapour concentrations from June, July and August for latitudes above 60°, the profile shown in Fig. 2 is obtained.

5 For temperature the MSISE-90 model (Hedin, 1991) is used as the apriori value. The model gives the mean temperature for each month as a function of latitude and pressure, covering pressures from 1013 hPa (~ 0 km) to  $5.7 \times 10^{-4}$  Pa (~ 130 km). Furthermore, the MSIS90E-90 climatology is used for the pressure–altitude relationship for the retrievals. However, since temperature, pressure and altitude are closely interlinked  
10 through the hydrostatic equilibrium (HSE), the pressure–altitude relationship must be adjusted during the retrieval to ensure a consistent relationship between the three variables. This is done by using the MSISE-90 model to find the geometrical altitude corresponding to a pressure level of 2.9 Pa, and the correcting the pressure–altitude relationship for the other pressure levels by assuming HSE in the retrieved atmosphere.

15 For the instrumental variables, the apriori assumption is that the measurements are correct i.e. a value of 0 is used for the frequency shift, pointing error the baseline fits.

## Retrieval of water vapour around PMCs from Odin-SMR

O. M. Christensen et al.

Title Page

Abstract

Introduction

Conclusions

References

Tables

Figures



Back

Close

Full Screen / Esc

Printer-friendly Version

Interactive Discussion



### 3.2.4 Apriori covariance

The optimal estimation method requires, in addition to apriori values, a covariance matrix to be created for the state vector variables. The total covariance matrix is set to a block diagonal matrix with the covariance matrix for each variable in each block

$$\mathbf{S}_a = \begin{pmatrix} \mathbf{S}_a^{\text{H}_2\text{O}} & 0 & 0 & 0 & 0 & 0 \\ 0 & \mathbf{S}_a^{\text{Temp}} & 0 & 0 & 0 & 0 \\ 0 & 0 & (\sigma_a^{\Delta F})^2 & 0 & 0 & 0 \\ 0 & 0 & 0 & (\sigma_a^{\Delta \theta})^2 & 0 & 0 \\ 0 & 0 & 0 & 0 & \mathbf{S}_a^{P0} & 0 \\ 0 & 0 & 0 & 0 & 0 & \mathbf{S}_a^{P1} \end{pmatrix}. \quad (3)$$

For the atmospheric fields the apriori covariance matrices are matrices with non zero elements far from the diagonal due to correlation in the errors in the apriori atmosphere and natural variation across the 2-D grid. In this study, following Eriksson (2000), we use two terms to describe this covariance. One term represents the large scale uncertainty of the apriori mean, whereas the other describes the smaller scale natural variations in the mesosphere (i.e. deviations from the true mean state). The apriori uncertainty for each of these terms is different. For water vapour and temperature, the SDs for the uncertainty in the apriori mean are set to 20% and 5 K, and the natural variability around the means are set to 20% and 10 K, respectively.

The spatial correlations of the uncertainty for these terms are also different, and to describe this we use correlation functions in both the vertical and horizontal directions. The correlation is modelled as a function,  $\rho$ , decreasing linearly with altitude/AAO. The correlation lengths,  $l_c$ , defined by  $\rho(l_c) = \exp^{-1}$ , are specified to 4° (20°) in the horizontal direction and 3 (8) km in the vertical direction for the natural variation (uncertainty in

## Retrieval of water vapour around PMCs from Odin-SMR

O. M. Christensen et al.

Title Page

Abstract

Introduction

Conclusions

References

Tables

Figures



Back

Close

Full Screen / Esc

Printer-friendly Version

Interactive Discussion



mean). The covariance for water vapour in the horizontal and vertical directions of the two terms and the total covariance is shown in Fig. 3a and b.

Assuming that the correlation in the two dimensions are independent (separable), the total correlation is given as the product of the two, and the complete covariance matrix can be calculated. A part of this matrix for water vapour is shown in Fig. 3a. It can be seen that the matrix has a block structure, where each block  $\mathbf{S}_a^{i,j}$ , indicated by the black square in the figure, is the covariance matrix covering all altitudes at one AAO, and the off-diagonal blocks are the vertical covariance matrix multiplied by the correlation between the different AAOs.

For the instrumental variables the covariance matrices are pure diagonal matrices (or scalars). For the baseline polynomial fits uncertainty is set to 4 and 2K for the zeroth and first order respectively. For the frequency fit the covariance matrix is simply a scalar with an assumed uncertainty of 100 kHz, whereas the pointing error the uncertainty is set to  $0.001^\circ$ . The strict regularisation on the pointing offset is needed to prevent the non-linear retrievals from converging to unrealistic results.

## 4 Results

### 4.1 A simulated case

In order to illustrate the viability of the tomographic methodology, a simulated retrieval was performed. In this way the sensitivity of the retrievals to changes in water vapour and temperature can be investigated. The mean temperature and water vapour retrieved from the tomographic measurements was used as the atmospheric a priori in the simulation. Since the purpose of this study is to look at small scale variations of water vapour and temperature around PMCs, a water vapour enhancement of 50% was simulated in a small region of the atmosphere (200 km  $\times$  2 km), and a set of simulated measurements were then generated using this atmosphere. This test atmosphere might not be realistic, but is a useful tool to qualitatively evaluating the performance

## Retrieval of water vapour around PMCs from Odin-SMR

O. M. Christensen et al.

Title Page

Abstract

Introduction

Conclusions

References

Tables

Figures



Back

Close

Full Screen / Esc

Printer-friendly Version

Interactive Discussion



## Retrieval of water vapour around PMCs from Odin-SMR

O. M. Christensen et al.

Title Page

Abstract

Introduction

Conclusions

References

Tables

Figures



Back

Close

Full Screen / Esc

Printer-friendly Version

Interactive Discussion



of the methodology. The retrieval was performed as described in Sect. 3. However, since the convergence criterion of the retrievals is based on changes from the a priori atmosphere, and only small deviations from the a priori atmosphere were simulated (compared to deviations expected in the real case), a stricter convergence criterion of 0.0001 had to be used in the simulated case, compared to 0.01 in the real retrievals. Furthermore, no noise was added to the simulated spectra, but the simulated retrievals were done using a noise covariance matrix describing a thermal noise with a  $\sigma$  of 2.6 K.

Figure 4a shows the retrieved water vapour, relative to the a priori atmosphere, from the simulated retrieval. The small area where the simulated atmosphere has enhanced water vapour is shown by the black contour, whereas the retrieved water vapour is shown by the coloured contours. It is clear from the results that the retrievals reproduce the water vapour enhancement, though some smoothing is seen as the area enhanced in the retrieved data is slightly larger than that of the simulated atmosphere.

In addition to water vapour, the tomographic retrieval returns the temperature field of the atmosphere. Due to the nature of the measurement method, these two retrieved quantities will not be independent of each other. As a result an increase in water vapour will have some influence on the retrieved temperature field, and Fig. 4b shows the change in retrieved temperature as a result of the water vapour enhancement. The temperature retrievals were affected by the enhancement in water vapour, and variations of  $\pm 3$  K are seen in the retrieved data around the water vapour enhancement.

To test the temperature retrievals, another simulation was set up. In this simulation (not shown) the water vapour distribution was set equal to the measured mean, and the temperature was perturbed by reducing it by 5 K in the 200 km  $\times$  2 km area. For the temperature the perturbed area was reproduced in the correct position, albeit with some smoothing. The influence on a change in temperature on the retrieved water vapour field was small, with a change of only 2% in the retrieved water vapour within the perturbed area, and no change outside of it.

The simulated tests show that the retrieval methodology is sound, and that the observations have the ability to detect small scale changes in water vapour in the area of



summer mesosphere where water vapour is brought up from the lower altitudes by the mesospheric overturning circulation and removed by photodissociation as it reaches the mesopause.

The latitudinal distribution of water vapour shows generally higher concentrations towards the pole than at lower latitudes, and both orbits have large areas with water vapour concentrations above 10 ppm between 70 and 80° N. Figure 6b in particular shows the water vapour concentrated in two areas at 80 and 100° AAO, while in Fig. 6a the concentration is highest at 100° AAO. These areas arise as a result of atmospheric dynamics combined with the redistribution of water vapour due to the presence of PMCs. Another feature of both figures is the wave like oscillating structures in the vertical directions seen across the entire orbit. These oscillations are retrieval artefacts due to thermal noise in the measurements, and do not represent the true structure of the atmosphere.

Below 80 km there are significant differences between the two orbits. Figure 6b shows less water vapour overall, and large amount of water between 65 and 105° AAO is not present compared to Fig. 6a. Comparing several other orbits show that this is probably due to instrumental differences between the two frontends rather than a physical change in the real atmosphere. The consequences and implication of this will be elaborated further in Sect. 5.3, where the results are compared to other satellite instruments.

Figure 7 shows the temperature field retrieved from orbit 51226. The retrieved temperature shows a mesopause altitude around 90 km with the lowest mesopause temperatures (~ 115 K) closest to the poles. This is once again due to the mesospheric overturning circulation, with the faster ascending air over the pole causing a stronger cooling than at lower latitudes.

**Retrieval of water vapour around PMCs from Odin-SMR**

O. M. Christensen et al.

Title Page	
Abstract	Introduction
Conclusions	References
Tables	Figures
◀	▶
◀	▶
Back	Close
Full Screen / Esc	
Printer-friendly Version	
Interactive Discussion	



## 5 Discussion

### 5.1 Averaging kernels

Spatial resolution of retrieved data is usually described by the rows of the averaging kernel matrix (AVKs). Each element in the averaging kernel matrix,  $\mathbf{A}_{ij}$ , gives the change in the retrieved state vector element  $\hat{x}_i$  from a change in the true state vector element  $x_j$ , and the spatial resolution of the retrievals can be described with the full width at half maximum (FWHM) of the AVKs.

For non-linear retrievals the AVKs will depend on the atmospheric state, and will vary between measurements. Thus, in order to give the most representative picture of the capabilities and limitation of the retrievals, we have chosen to show the AVKs using the mean retrieved state from all the measurements. The AVKs are calculated assuming that the Levenberg–Marquard parameter is zero at the final iteration, i.e. we present the AVKs for the linear retrieval around the mean retrieved atmospheric state (Ceccherini and Ridolfi, 2010). This is valid for most of the retrieved cases, although for some batches the Levenberg–Marquard parameter does not reach zero, but remains between 1 to 4 during the final iterations. For these batches, the AVKs presented here should be regarded as an approximation, rather than a perfect characterisation of the performance of the retrievals.

#### 5.1.1 Spatial resolution

Figure 8 shows the calculated horizontal and vertical averaging kernels. The vertical AVKs show a clear separation between the different altitudes for both water vapour and temperature, and between 75–88 km and the vertical resolution is 2.5 km. The horizontal AVKs for different altitudes are shown in left panels of Fig. 8. The horizontal AVKs have a more jagged appearance than the vertical ones, and their peaks do not always align with the AAO which they represent. However, for the altitudes between 74–81 km a clear peak with a FWHM of  $\sim 2^\circ$  (220 km) can be seen. The horizontal

## Retrieval of water vapour around PMCs from Odin-SMR

O. M. Christensen et al.

Title Page

Abstract

Introduction

Conclusions

References

Tables

Figures



Back

Close

Full Screen / Esc

Printer-friendly Version

Interactive Discussion



AVKs do oscillate, and a secondary peak is seen  $\sim 4^\circ$  on either side of the main peak. At higher altitudes (83 and 85 km) the main peak is less pronounced and the AVK is a flatter with FWHM of up to  $5^\circ$ . This shows that the best horizontal resolutions are for the altitudes around 80 km, with a deteriorating resolution as the altitude increases.

### 5.1.2 Measurement response

The measurement response (MR) of the retrievals gives an indication of how sensitive the retrievals are to large scale changes in the true atmosphere, and is calculated by summing the AVKs along each row over all columns corresponding to the retrieved variable (Baron et al., 2002). The measurement response (MR) for water vapour and temperature are shown as solid lines in Fig. 8a and c respectively. The plotted value is the measurement response/10, and altitudes with values greater than  $\sim 0.6$  are areas where the measurement information is considered to contribute significantly to the retrieved data. This area covers the altitudes between 75 and 90 km. The retrieved large scale changes, however, have large uncertainties. These errors come from the fact that there is little information about the ambient pressure of the atmosphere in the measured radiation. The result of this is that errors in the pointing of the satellite as well as errors in the altitude of the HSE reference pressure level of the retrievals can lead to large errors in the retrieved water vapour mixing ratio (see Sect. 5.2). An alternative measurement response is therefore calculated to show the sensitivity of the retrievals to smaller scale changes in the atmosphere. It is calculated by summing over the AVK columns from a  $4^\circ$  latitude band around the corresponding state vector element, and is shown by the dashed lines in Fig. 8a and c. For temperature, this measurement response is similar to the one for large scale changes, whereas for water vapour the measurement response is reduced at altitudes above 85 km.

## Retrieval of water vapour around PMCs from Odin-SMR

O. M. Christensen et al.

Title Page

Abstract

Introduction

Conclusions

References

Tables

Figures



Back

Close

Full Screen / Esc

Printer-friendly Version

Interactive Discussion



## 5.2 Errors

There are several possible sources of errors in the retrievals. Random errors come from thermal noise in the measurements (retrieval noise), from the limited resolution of the measurements (smoothing error), and pointing error in the satellite. Additionally, the results have systematic errors related to uncertainties in modelling of the instrument, modelling of the atmosphere, and uncertainties in the spectral line parameters. Just as with the averaging kernels, the effect of uncertainties and errors will depend on the true atmospheric profile. Thus, to give an indication of the average error expected in the retrievals, the error analysis is based around a case linearised around the mean retrieved state of the measurements.

The smoothing error and retrieval noise are calculated using the covariance matrices,  $\mathbf{S}_a$  and  $\mathbf{S}_e$  respectively, as described in Rodgers (2000). The retrieval noise is  $\sim 0.5$  ppm for water vapour and 3 K for temperature. An accurate estimation of the smoothing error, however, requires that the atmospheric covariance matrix is known with certainty, which is not the case for the tomographic retrievals. As such we will not use the smoothing errors for the error analysis, but rather consider the retrieved result as the smoothed version of the true atmosphere, with the resolution given by the averaging kernels.

For the systematic errors, their influence is estimated by performing a simulated retrieval on the mean retrieved state with the forward model perturbed to the  $\pm 1\sigma$  estimate of the investigated parameter. The parameters investigated are the linestrength,  $I_0$ , which is perturbed  $\pm 2\%$ , based on the JPL uncertainty, the pressure broadening parameter,  $\gamma$ , which is perturbed 5%, based on differences between the measurements reported in Seta et al. (2008). Errors in the altitude of the HSE reference pressure level (2.9 Pa), *Pressure*, is estimated by moving the pressure level  $\pm 2$  km, based on differences between MSISE90 and CIRA86 (Fleming et al., 1990) at 70 km. Additionally uncertainties related to the properties of the SMR instrument are simulated. The

## Retrieval of water vapour around PMCs from Odin-SMR

O. M. Christensen et al.

Title Page

Abstract

Introduction

Conclusions

References

Tables

Figures



Back

Close

Full Screen / Esc

Printer-friendly Version

Interactive Discussion



instrumental parameters investigated are an offset in the pointing of  $\pm 0.02^\circ$  (Lossow et al., 2007), and uncertainties in the sideband suppression of  $\pm 2\%$  (11–15 dB).

It should be noted that the presence of PMCs will not affect the retrieval of water vapour and temperature from SMR. The radiance emitted from ice particles is in the order of 0.1 K, and will be very uniform across the bandwidth of the spectrometer. As such, it will be completely overshadowed by any baseline in spectrometer, and thus corrected for in the polynomial baseline fit performed on each spectrum.

Figure 9 shows the random and systematic errors estimated around the mean atmospheric state. The plotted value,  $\Delta E$ , is the mean absolute value of the difference between the perturbed,  $x(\pm\sigma)$ , and unperturbed,  $x(0)$ , retrievals given by

$$\Delta E = \frac{|x(\sigma) - x(0)| + |x(-\sigma) - x(0)|}{2}. \quad (4)$$

The two largest sources of uncertainties in the retrievals are the pressure–altitude relationship (red line) and errors in pointing of the satellite (cyan line). The reason for this is that the weighting function for a change in water vapour is similar to the weighting function from the changing of the pointing angle of the satellite, or from a change in ambient pressure at different altitudes. Since the water vapour line is dominated by Doppler (compared to pressure-) broadening at the observed altitudes, and the number density of molecules decrease exponentially with altitude, any pointing error (or errors in altitude of the HSE reference point) will give rise to a large scale change in the retrieved water vapour mixing ratio, and vice versa. The errors arising from assuming the wrong altitude of the 2.9 Pa pressure level can be adjusted for by ensuring that comparisons to other instruments or models are done with respect to a common pressure vs. altitude profile, in effect comparing number density- rather than mixing ratio profiles. If this is done, the estimated systematic error from this uncertainty is lowered to  $\sim 2$  ppm (red-dashed curve in Fig. 9).

The uncertainties from the two aforementioned errors (*Pointing* and *Pressure*) are however highly correlated across each orbit and will mainly affect the mean water

## Retrieval of water vapour around PMCs from Odin-SMR

O. M. Christensen et al.

[Title Page](#)[Abstract](#)[Introduction](#)[Conclusions](#)[References](#)[Tables](#)[Figures](#)[Back](#)[Close](#)[Full Screen / Esc](#)[Printer-friendly Version](#)[Interactive Discussion](#)

## Retrieval of water vapour around PMCs from Odin-SMR

O. M. Christensen et al.

Title Page

Abstract

Introduction

Conclusions

References

Tables

Figures



Back

Close

Full Screen / Esc

Printer-friendly Version

Interactive Discussion



vapour field retrieved in each orbit, and not the variations around this field. For these variations the other systematic errors will dominate, and as these are on the order of the noise in the data, we conclude that the measurements reliably can retrieve these variations, despite the poor accuracy of the mean field. It should also be noted that the systematic errors introduced from the pointing and pressure uncertainties do not necessarily lead to a bias as both errors may vary across the measurement period.

### 5.3 Comparison with other measurements

As a final test of the ability of the observations to retrieve water vapour and temperature, the results are compared to measurements from other satellite instruments. The solar occulting instruments Atmospheric Chemistry Experiment-Fourier Transform Spectrometer (ACE-FTS) on board the SCISAT satellite (Bernath et al., 2005) and Solar Occultation for Ice Experiment (SOFIE) on board the AIM satellite (Russell et al., 2009) provide water vapour and temperature measurements with high vertical resolution in the area covered by the tomographic retrievals during the time period of the tomographic measurements.

ACE-FTS is a Fourier transform spectrometer which measures solar radiation between  $750\text{--}4400\text{ cm}^{-1}$  and retrieves water vapour and temperature profiles (Boone et al., 2005) between 5–90 km with an altitude resolution of 3–4 km and a precision of  $\sim 300$  ppbv for water vapour (statistical fitting error and “form-factor” error Boone et al., 2013) and  $\sim 2$  K for temperature (comparison to LIDAR Sica et al., 2008). In this study we use version 3.0 of the water vapour data (Boone et al., 2013), which provides data during July 2010 in the time period covered by tomographic retrievals.

SOFIE uses differential absorption spectroscopy at eleven different wavelengths between  $0.292$  to  $5.316\ \mu\text{m}$  to determine the temperature and the atmospheric composition. It retrieves water vapour and temperature between 20–95 km with a vertical resolution of 1–2 km. The precision for water vapour is estimated to be better than 0.2 ppmv across the mesopause (Rong et al., 2010), and for temperature the precision is estimated to 0.1 K at 80 km increasing up to 0.5 K at 95 km (Stevens et al., 2012). In



graphic measurements successfully can retrieve water vapour and temperature structures in the area of interest.

To look at the systematic errors in the tomographic retrievals, the mean of all measurements collocated with SOFIE is analysed. A total of 198 collocations are investigated, and Fig. 11a and b shows the result of this comparison with respect to each of the two frequency modes of SMR. The measurements using mode 19 show a low bias compared to SOFIE in both water vapour ( $> 1$  ppm) and temperature ( $> 20$  K). These biases are also seen in the measurements using mode 13, but they are significantly smaller. The estimated accuracy of SOFIE is  $\sim 5\%/0.8$  K at 80 km and  $15\%/9.9$  K at 95 km for water vapour (Rong et al., 2010) and temperature (Stevens et al., 2012) respectively. Taking this into account the agreement between SMR and SOFIE is good for mode 13, but not for mode 19. Above 90 km a large difference in mean temperature can be seen. However, this is probably due to a known high bias in SOFIE (Stevens et al., 2012).

The comparison of the mean profiles can be extended by looking at the mean profile from each month for SOFIE and SMR. Figure 11c shows the mean water vapour profiles from both instruments for June, July and August averaged over 2010 and 2011. Only the collocations from the frequency mode 13 measurements are used. In June, SOFIE (blue-dashed line) shows a higher water vapour concentration below 82 km than SMR (blue line), while in August (red lines) the reverse is true. The reason for the larger seasonal variation in water vapour in SMR is unknown, but it could be linked to systematic errors in the pressure a priori used for the retrievals. The mean temperature (Fig. 11d) is very similar for both SMR and SOFIE for June and July, while for August SOFIE retrieves a much higher mesopause temperature (155 K) compared to SMR (140 K).

It should be noted that the measured water vapour mixing ratios are first converted to number density, before they are rescaled using a common pressure and temperature profile during the comparisons. This means that in principle number density profiles are compared rather than mixing ratios. Doing this mitigates errors arising from the lack of

## Retrieval of water vapour around PMCs from Odin-SMR

O. M. Christensen et al.

[Title Page](#)[Abstract](#)[Introduction](#)[Conclusions](#)[References](#)[Tables](#)[Figures](#)[Back](#)[Close](#)[Full Screen / Esc](#)[Printer-friendly Version](#)[Interactive Discussion](#)



trate into areas of higher temperature ( $> 150$  K), once again explaining these intrusions require further analysis taking into account both cloud microphysics and the dynamics of the atmosphere.

## 6 Conclusions

Water vapour and temperature have been measured around PMC by several ground- and satellite based instruments in the past, but until now, simultaneous measurements of water vapour, temperature and PMC with a large geographical coverage and relatively good vertical and horizontal resolution have not existed. During the arctic summers of 2010, 2011 and 2014 the Odin satellite made a set of measurements with both Odin-SMR and Odin-OSIRIS to obtain such data.

In this paper we present the measurements of water vapour and temperature carried out by the SMR instrument. A tomographic retrieval approach based on the optimal estimation method is applied, and is described in detail. An error analysis was performed to investigate possible sources of errors in the retrieved data, and the data was compared to two other satellite instruments for quality assurance.

The largest source of errors in the data comes from the uncertainty in the satellite pointing and the altitude of the 2.9 Pa pressure level, which is used as the reference level to adjust the atmosphere to remain in HSE. These large uncertainties indicate that the tomographic retrievals have limited capability to retrieve the mean water vapour mixing ratio for each orbit. However, the retrieved variations of water vapour around this mean are significantly less affected by these errors, and can be retrieved by the measurements with reasonable accuracy.

Inspecting tomographic retrievals done in different frequency modes revealed discrepancies between measurements frequency mode 19 and 13. By comparing the results to collocated AIM-SOFIE measurements, we conclude that the best results are achieved with the frequency mode 13 measurements, which had the lowest systematic differences compared to AIM-SOFIE of the two modes. A larger seasonal variation in

## Retrieval of water vapour around PMCs from Odin-SMR

O. M. Christensen et al.

Title Page

Abstract

Introduction

Conclusions

References

Tables

Figures



Back

Close

Full Screen / Esc

Printer-friendly Version

Interactive Discussion



---

**Retrieval of water vapour around PMCs from Odin-SMR**O. M. Christensen et al.

---

[Title Page](#)[Abstract](#)[Introduction](#)[Conclusions](#)[References](#)[Tables](#)[Figures](#)[Back](#)[Close](#)[Full Screen / Esc](#)[Printer-friendly Version](#)[Interactive Discussion](#)

water vapour was also found in SMR compared to AIM-SOFIE. The reason for these discrepancies are not clear, but are probably a combination of errors in the modelling of the SMR instrument, and errors in assumptions about the forward model atmosphere.

Despite these uncertainties, the SMR tomographic measurements provide a unique and useful complement to existing datasets. As an example of the capabilities of the measurements, we compared the retrieved atmosphere to PMC extinction coefficients measured by OSIRIS for two of the recorded orbits. The results from the two instruments showed both depletion and enhancement of water vapour around the clouds as well as larger scale horizontal variation in both water vapour and temperature. To explain the complete water vapour and temperature fields of the background atmosphere requires a more thorough analysis, taking into account both cloud microphysics as well as atmospheric dynamics. Future plans include using the dataset to evaluate atmospheric and cloud models, and thus improve our understanding of PMCs and their effect on and response to the background atmosphere under which they form.

*Acknowledgements.* We would like to thank Kaley Walker and the ACE-FTS/SCISAT team as well as Mark Hervig and the SOFIE/AIM team for providing satellite data of water vapour and temperature for comparison.

The Atmospheric Chemistry Experiment (ACE), also known as SCISAT, is a Canadian-led mission mainly supported by the Canadian Space Agency and the Natural Sciences and Engineering Research Council of Canada.

AIM/SOFIE is funded by NASA's Small Explorers Program. The SOFIE v1.2 data used in this work are available online at [sofie.gats-inc.com](http://sofie.gats-inc.com).

Odin is a Swedish-led satellite project funded jointly by the Swedish National Space Board (SNSB), the Canadian Space Agency (CSA), the National Technology Agency of Finland (Tekes), the Centre National d'études Spatiales (CNES) in France and the European Space Agency (ESA).

## References

- Baron, P., Ricaud, P., de la Noë, J., Eriksson, P., Merino, F., and Murtagh, D.: Studies for the Odin sub-millimetre radiometer: retrieval methodology, *Can. J. Phys.*, 80, 341–356, 2002. 11873
- 5 Bernath, P. F., McElroy, C. T., Abrams, M. C., Boone, C. D., Butler, M., Camy-Peyret, C., Carleer, M., Clerbaux, C., Coheur, P.-F., Colin, R., DeCola, P., DeMazière, M., Drummond, J. R., Dufour, D., Evans, W. F. J., Fast, H., Fussen, D., Gilbert, K., Jennings, D. E., Llewellyn, E. J., Lowe, R. P., Mahieu, E., McConnell, J. C., McHugh, M., McLeod, S. D., Michaud, R., Midwinter, C., Nassar, R., Nichitiu, F., Nowlan, C., Rinsland, C. P., Rochon, Y. J., Rowlands, N., Semeniuk, K., Simon, P., Skelton, R., Sloan, J. J., Soucy, M.-A., Strong, K., Tremblay, P., Turnbull, D., Walker, K. A., Walkty, I., Wardle, D. A., Wehrle, V., Zander, R., and Zou, J.: Atmospheric chemistry experiment (ACE): mission overview, *Geophys. Res. Lett.*, 32, L15S01, doi:10.1029/2005GL022386, 2005. 11876
- 10 Boone, C. D., Nassar, R., Walker, K. A., Rochon, Y., McLeod, S. D., Rinsland, C. P., and Bernath, P. F.: Retrievals for the atmospheric chemistry experiment Fourier-transform spectrometer, *Appl. Optics*, 44, 7218–7231, doi:10.1364/AO.44.007218, 2005. 11876
- 15 Boone, C. D., Walker, K. A., and Bernath, P. F.: Retrievals for the Atmospheric Chemistry Experiment Fourier Transform Spectrometer (ACE-FTS), in: *The Atmospheric Chemistry Experiment ACE at 10: A Solar Occultation Anthology*, edited by: Bernath, P. F., A. Deepak Publishing, Hampton, Virginia, USA, 2013. 11876
- 20 Buehler, S. A., Eriksson, P., Kuhn, T., von Engeln, A., and Verdes, C.: ARTS, the Atmospheric Radiative Transfer Simulator, *J. Quant. Spectrosc. Ra.*, 91, 65–93, 2005. 11861
- Ceccherini, S. and Ridolfi, M.: Technical Note: Variance-covariance matrix and averaging kernels for the Levenberg-Marquardt solution of the retrieval of atmospheric vertical profiles, *Atmos. Chem. Phys.*, 10, 3131–3139, doi:10.5194/acp-10-3131-2010, 2010. 11872
- 25 Degenstein, D. A., Llewellyn, E. J., and Lloyd, N. D.: Volume emission rate tomography from a satellite platform, *Appl. Optics*, 42, 1441–1450, 2003. 11857, 11861
- Eriksson, P.: Analysis and comparison of two linear regularization methods for passive atmospheric observations, *J. Geophys. Res.*, 105, 18157–18167, doi:10.1029/2000JD900172, 2000. 11867
- 30

AMTD

7, 11853–11900, 2014

## Retrieval of water vapour around PMCs from Odin-SMR

O. M. Christensen et al.

Title Page

Abstract

Introduction

Conclusions

References

Tables

Figures



Back

Close

Full Screen / Esc

Printer-friendly Version

Interactive Discussion



---

**Retrieval of water vapour around PMCs from Odin-SMR**O. M. Christensen et al.

---

[Title Page](#)[Abstract](#)[Introduction](#)[Conclusions](#)[References](#)[Tables](#)[Figures](#)[Back](#)[Close](#)[Full Screen / Esc](#)[Printer-friendly Version](#)[Interactive Discussion](#)

Eriksson, P., Merino, F., Murtagh, D., Baron, P., Ricaud, P., and de la Noë, J.: Studies for the Odin sub-millimetre radiometer: 1. Radiative transfer and instrument simulation, *Can. J. Phys.*, 80, 321–340, 2002. 11859, 11864

Eriksson, P., Ekström, M., Bühler, S. A., and Melsheimer, C.: Efficient forward modelling by matrix representation of sensor responses, *Int. J. Remote Sens.*, 27, 1793–1808, 2006. 11864

Eriksson, P., Bühler, S., Davis, C., Emde, C., and Lemke, O.: ARTS, the atmospheric radiative transfer simulator, version 2, *J. Quant. Spectrosc. Ra.*, 112, 1551–1558, doi:10.1016/j.jqsrt.2011.03.001, 2011. 11861

Feofilov, A. G., Kutepov, A. A., Pesnell, W. D., Goldberg, R. A., Marshall, B. T., Gordley, L. L., García-Comas, M., López-Puertas, M., Manuilova, R. O., Yankovsky, V. A., Petelina, S. V., and Russell III, J. M.: Daytime SABER/TIMED observations of water vapor in the mesosphere: retrieval approach and first results, *Atmos. Chem. Phys.*, 9, 8139–8158, doi:10.5194/acp-9-8139-2009, 2009. 11856

Fleming, E. L., Chandra, S., Barnett, J., and Corney, M.: Zonal mean temperature, pressure, zonal wind and geopotential height as functions of latitude, *Adv. Space Res.*, 10, 11–59, doi:10.1016/0273-1177(90)90386-E, 1990. 11874

Frisk, U., Hagström, M., Ala-Laurinaho, J., Andersson, S., Berges, J.-C., Chabaud, J.-P., Dahlgren, M., Emrich, A., Florén, H.-G., Florin, G., Fredrixon, M., Gaier, T., Haas, R., Hirvonen, T., Hjalmarsson, Å., Jakobsson, B., Jukkala, P., Kildal, P. S., Kollberg, E., Lassing, E., Lecacheux, A., Lehikoinen, P., Lehto, A., Mallat, J., Marty, C., Michet, D., Narbonne, J., Nexon, M., Olberg, M., Olofsson, A. O. H., Olofsson, G., Origné, A., Petersson, M., Piironen, P., Pons, R., Pouliquen, D., Ristorcelli, I., Rosolen, C., Rouaix, G., Räisänen, A. V., Serra, G., Sjöberg, F., Stenmark, L., Torchinsky, S., Tuovinen, J., Ullberg, C., Vinterhav, E., Wade-falk, N., Zirath, H., Zimmermann, P., and Zimmermann, R.: The Odin satellite. I. Radiometer design and test, *Astron. Astrophys.*, 402, L27–L34, 2003. 11859, 11860

Hedin, A. E.: Extension of the MSIS thermosphere model into the middle and lower atmosphere, *J. Geophys. Res.*, 96, 1159–1172, doi:10.1029/90JA02125, 1991. 11866

Hervig, M. E., Stevens, M. H., Gordley, L. L., Deaver, L. E., Russell, J. M., and Bailey, S. M.: Relationships between polar mesospheric clouds, temperature, and water vapor from Solar Occultation for Ice Experiment (SOFIE) observations, *J. Geophys. Res.*, 114, D20203, doi:10.1029/2009JD012302, 2009. 11855

Hultgren, K., Gumbel, J., Degenstein, D., Bourassa, A., Lloyd, N., and Stegman, J.: First simultaneous retrievals of horizontal and vertical structures of Polar Meso-

## Retrieval of water vapour around PMCs from Odin-SMR

O. M. Christensen et al.

Title Page

Abstract

Introduction

Conclusions

References

Tables

Figures



Back

Close

Full Screen / Esc

Printer-friendly Version

Interactive Discussion



spheric Clouds from Odin/OSIRIS tomography, *J. Atmos. Sol.-Terr. Phys.*, 104, 213–223, doi:10.1016/j.jastp.2013.06.013, 2013. 11857, 11861

Lübken, F.-J., Jarvis, M. J., and Jones, G. O. L.: First in situ temperature measurements at the Antarctic summer mesopause, *Geophys. Res. Lett.*, 26, 3581–3584, doi:10.1029/1999GL010719, 1999. 11855

Livesey, N., Van Snyder, W., Read, W., and Wagner, P.: Retrieval algorithms for the EOS Microwave limb sounder (MLS), *IEEE T. Geosci. Remote*, 44, 1144–1155, doi:10.1109/TGRS.2006.872327, 2006. 11857

Lossow, S., Urban, J., Eriksson, P., Murtagh, D., and Gumbel, J.: Critical parameters for the retrieval of mesospheric water vapour and temperature from Odin/SMR limb measurements at 557 GHz, *Adv. Space Res.*, 40, 835–845, 2007. 11856, 11858, 11859, 11875

Lossow, S., Urban, J., Schmidt, H., Marsh, D., Gumbel, J., Eriksson, P., and Murtagh, D.: Wintertime water vapor in the polar upper mesosphere and lower thermosphere: first satellite observations by Odin submillimeter radiometer, *J. Geophys. Res.*, 114, D10304, doi:10.1029/2008JD011462, 2009. 11856

López-Puertas, M., García-Comas, M., Funke, B., Bermejo-Pantaleón, D., Höpfner, M., Grabowski, U., Stiller, G. P., von Clarmann, T., and von Savigny, C.: Measurements of polar mesospheric clouds in infrared emission by MIPAS/ENVISAT, *J. Geophys. Res.*, 114, D00107, doi:10.1029/2009JD012548, 2009. 11856

Lübken, F.-J., Rapp, M., and Strelnikova, I.: The sensitivity of mesospheric ice layers to atmospheric background temperatures and water vapor, *Adv. Space Res.*, 40, 794–801, 2007. 11855

McHugh, M., Hervig, M., Magill, B., Thompson, R. E., Remsberg, E., Wrotny, J., and Russell III, J.: Improved mesospheric temperature, water vapor and polar mesospheric cloud extinctions from HALOE, *Geophys. Res. Lett.*, 30, 1440, doi:10.1029/2002GL016859, 2003. 11855

Murtagh, D., Frisk, U., Merino, F., Ridal, M., Jonsson, A., Stegman, J., Witt, G., Eriksson, P., Jiménez, C., Megie, G., de la Noë, J., Ricaud, P., Baron, P., Pardo, J. R., Hauchcorne, A., Llewellyn, E. J., Degenstein, D. A., Gattinger, R. L., Lloyd, N. D., Evans, W. F. J., McDade, I. C., Haley, C., Sioris, C., von Savigny, C., Solheim, B. H., McConnell, J. C., Strong, K., Richardson, E. H., Leppelmeier, G. W., Kyrölä, E., Auvinen, H., and Oikarinen, L.: An overview of the Odin atmospheric mission, *Can. J. Phys.*, 80, 309–319, 2002. 11858

## Retrieval of water vapour around PMCs from Odin-SMR

O. M. Christensen et al.

Title Page

Abstract

Introduction

Conclusions

References

Tables

Figures



Back

Close

Full Screen / Esc

Printer-friendly Version

Interactive Discussion



Pickett, H., Poynter, R., Cohen, E., Delitsky, M., Pearson, J., and Muller, H.: Submillimeter, millimeter, and microwave spectral line catalog, *J. Quant. Spectrosc. Rad.*, 60, 883–890, 1998. 11863

Pukite, J., Kühl, S., Deutschmann, T., Platt, U., and Wagner, T.: Accounting for the effect of horizontal gradients in limb measurements of scattered sunlight, *Atmos. Chem. Phys.*, 8, 3045–3060, doi:10.5194/acp-8-3045-2008, 2008. 11857

Rapp, M. and Thomas, G. E.: Modeling the microphysics of mesospheric ice particles: assessment of current capabilities and basic sensitivities, *J. Atmos. Sol.-Terr. Phys.*, 68, 715–744, 2006. 11855

Rodgers, C.: *Inverse Methods for Atmospheric Sounding: Theory and Practice*, World Scientific, Singapore, 2000. 11864, 11874

Rong, P., Russell, J. M., Gordley, L. L., Hervig, M. E., Deaver, L., Bernath, P. F., and Walker, K. A.: Validation of v1. 022 mesospheric water vapor observed by the Solar Occultation for Ice Experiment instrument on the Aeronomy of Ice in the Mesosphere satellite, *J. Geophys. Res.*, 115, D24314, doi:10.1029/2010JD014269, 2010. 11876, 11878

Rong, P., Russell, J., Hervig, M., and Bailey, S.: The roles of temperature and water vapor at different stages of the polar mesospheric cloud season, *J. Geophys. Res.*, 117, D04208, doi:10.1029/2011JD016464, 2012. 11855

Rong, P. P., Russell, J. M., Randall, C. E., Bailey, S. M., and Lambert, A.: Northern PMC brightness zonal variability and its correlation with temperature and water vapor, *J. Geophys. Res.-Atmos.*, 119, 2390–2408, doi:10.1002/2013JD020513, 2014. 11856

Rothman, L. S., Gordon, I. E., Babikov, Y., Barbe, A., Chris Benner D., Bernath, P. F., Birk, M., Bizzocchi, L., Boudon, V., Brown, L. R., Campargue, A., Chance, K., Cohen, E. A., Coudert, L. H., Devi, V. M., Drouin, B. J. Fayt, A., Flaud, J.-M., Gamache, R. R., Harrison, J. J., Hartmann, J.-M., Hill, C., Hodges, J. T., Jacquemart, D., Jolly, A., Lamouroux, J., Le Roy, R. J., Li, G., Long, D. A., Lyulin, O. M., Mackie, C. J., Massie, S. T., Mikhailenko, S., Müller, H. S. P., Naumenko, O. V., Nikitin, A. V., Orphal, J., Perevalov, V., Perrin, A., Polovtseva, E. R., Richard, C., Smith, M. A. H., Starikova, E., Sung, K., Tashkun, S., Tennyson, J., Toon, G. C., Tyuterev, V. G., and Wagner, G.: The HITRAN2012 molecular spectroscopic database, *J. Quant. Spectrosc. Ra.*, 130, 4–50, doi:10.1016/j.jqsrt.2013.07.002, 2013. 11863

Russell, J. M., Bailey, S. M., Gordley, L. L., Rusch, D. W., Horányi, M., Hervig, M. E., Thomas, G. E., Randall, C. E., Siskind, D. E., Stevens, M. H., Summers, M. E., Taylor, M. J., Englert, C. R., Espy, P. J., McClintock, W. E., and Merkel, A. W.: The Aeronomy of Ice in the Mesosphere

**Retrieval of water vapour around PMCs from Odin-SMR**

O. M. Christensen et al.

Title Page

Abstract

Introduction

Conclusions

References

Tables

Figures



Back

Close

Full Screen / Esc

Printer-friendly Version

Interactive Discussion



(AIM) mission: overview and early science results, *J. Atmos. Sol.-Terr. Phys.*, 71, 289–299, doi:10.1016/j.jastp.2008.08.011, 2009. 11855, 11876

Seele, C. and Hartogh, P.: Water vapor of the polar middle atmosphere: annual variation and summer mesosphere conditions as observed by ground-based microwave spectroscopy, *Geophys. Res. Lett.*, 26, 1517–1520, doi:10.1029/1999GL900315, 1999. 11855

Seta, T., Hoshina, H., Kasai, Y., Hosako, I., Otani, C., Lossow, S., Urban, J., Ekström, M., Eriksson, P., and Murtagh, D. P.: Pressure broadening coefficients of the water vapor lines at 556.936 and 752.033 GHz, *J. Quant. Spectrosc. Rad.*, 109, 144–150, 2008. 11874

Sheese, P. E., Llewellyn, E. J., Gattinger, R. L., Bourassa, A. E., Degenstein, D. A., Lloyd, N. D., and McDade, I. C.: Mesopause temperatures during the polar mesospheric cloud season, *Geophys. Res. Lett.*, 38, L11803, doi:10.1029/2011GL047437, 2011. 11855

Sica, R. J., Izawa, M. R. M., Walker, K. A., Boone, C., Petelina, S. V., Argall, P. S., Bernath, P., Burns, G. B., Catoire, V., Collins, R. L., Daffer, W. H., De Clercq, C., Fan, Z. Y., Firanski, B. J., French, W. J. R., Gerard, P., Gerding, M., Granville, J., Innis, J. L., Keckhut, P., Kerzenmacher, T., Klekociuk, A. R., Kyrö, E., Lambert, J. C., Llewellyn, E. J., Manney, G. L., McDermid, I. S., Mizutani, K., Murayama, Y., Piccolo, C., Raspollini, P., Ridolfi, M., Robert, C., Steinbrecht, W., Strawbridge, K. B., Strong, K., Stübi, R., and Thurairajah, B.: Validation of the Atmospheric Chemistry Experiment (ACE) version 2.2 temperature using ground-based and space-borne measurements, *Atmos. Chem. Phys.*, 8, 35–62, doi:10.5194/acp-8-35-2008, 2008. 11876

Steck, T., Höpfner, M., von Clarmann, T., and Grabowski, U.: Tomographic retrieval of atmospheric parameters from infrared limb emission observations, *Appl. Optics*, 44, 3291–3301, doi:10.1364/AO.44.003291, 2005. 11857

Stevens, M. H., Deaver, L. E., Hervig, M. E., Russell, J. M., Siskind, D. E., Sheese, P. E., Llewellyn, E. J., Gattinger, R. L., Höpfner, J., and Marshall, B.: Validation of upper mesospheric and lower thermospheric temperatures measured by the Solar Occultation for Ice Experiment, *J. Geophys. Res.*, 117, D16304, doi:10.1029/2012JD017689, 2012. 11876, 11878

Thomas, G. E., Olivero, J. J., Jensen, E. J., Schroeder, W., and Toon, O. B.: Relation between increasing methane and the presence of ice clouds at the mesopause, *Nature*, 338, 490–492, 1989. 11855

Thomas, G. E., Olivero, J. J., Deland, M., and Shettle, E. P. E. P.: Comment on “Are noctilucent clouds truly a “Miner’s Canary” for Global Change?”, *Eos T. Am. Geophys. Un.*, 84, 352–353, 2003. 11855

von Zahn, U.: Are noctilucent clouds a “Miner’s Canary” for global change?, *Eos T. Am. Geophys. Un.*, 84, 261–264, doi:10.1029/2003EO280001, 2003. 11855

Zasetsky, A., Petelina, S., Remorov, R., Boone, C., Bernath, P., and Llewellyn, E.: Ice particle growth in the polar summer mesosphere: formation time and equilibrium size, *Geophys. Res. Lett.*, 36, L15803, doi:10.1029/2009GL038727, 2009. 11855

## AMTD

7, 11853–11900, 2014

### Retrieval of water vapour around PMCs from Odin-SMR

O. M. Christensen et al.

Title Page

Abstract

Introduction

Conclusions

References

Tables

Figures



Back

Close

Full Screen / Esc

Printer-friendly Version

Interactive Discussion





## Retrieval of water vapour around PMCs from Odin-SMR

O. M. Christensen et al.

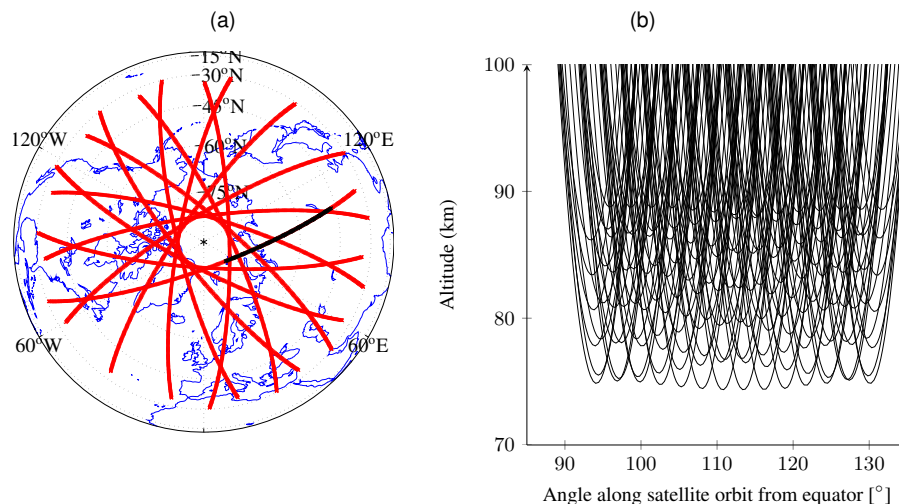


**Figure 1.** (a) Coverage of SMR tomographic measurements 16 July 2010. The red points are the tangent positions for each spectrum. The spectra are retrieved in processed in batches of 150 spectra, the tangent positions for the spectra in one such batch are shown by the black points. (b) The line-of-sight through the atmosphere for the measurements marked by the black points in (a).

Title Page

Abstract

Introduction

Conclusions

References

Tables

Figures



Back

Close

Full Screen / Esc

Printer-friendly Version

Interactive Discussion



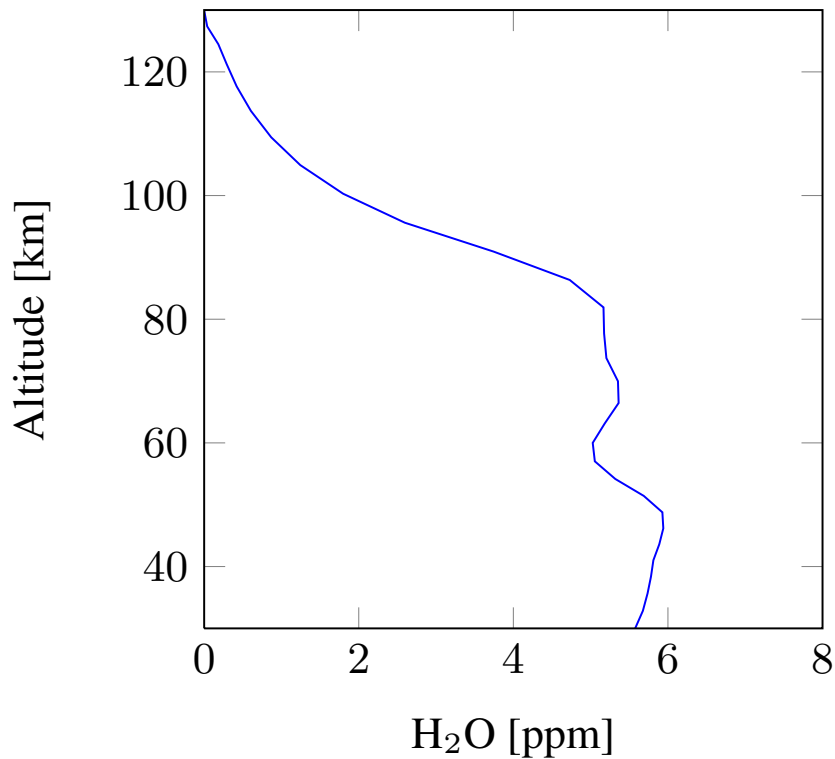


**Figure 2.** The H<sub>2</sub>O apriori profile created from the mean of a MLS climatology.

**Retrieval of water vapour around PMCs from Odin-SMR**

O. M. Christensen et al.

Title Page	
Abstract	Introduction
Conclusions	References
Tables	Figures
◀	▶
◀	▶
Back	Close
Full Screen / Esc	
Printer-friendly Version	
Interactive Discussion	



## Retrieval of water vapour around PMCs from Odin-SMR

O. M. Christensen et al.

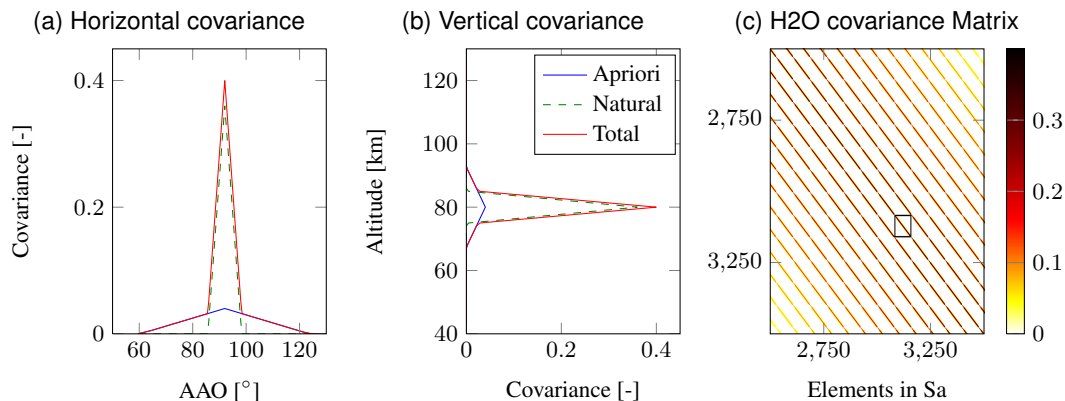


**Figure 3.** (a) Vertical and (b) horizontal elements of the covariance matrix for H<sub>2</sub>O. The blue line is the uncertainty of the apriori mean values, the green dashed line the natural variability of water vapour around the apriori mean, and the red line is the total covariance. (c) Elements of the total covariance matrix for water vapour. The black square indicates a single covariance block, i.e. covariance between altitudes at the same AAO.



## Retrieval of water vapour around PMCs from Odin-SMR

O. M. Christensen et al.

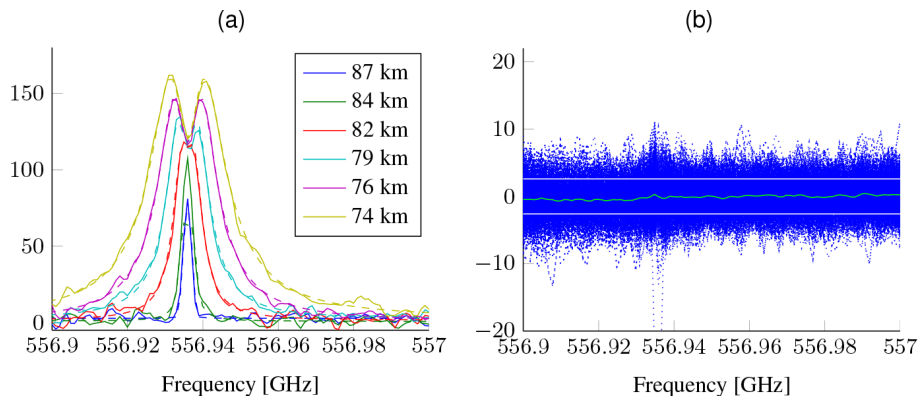


**Figure 5.** (a) Sample spectra of the 557 GHz line from orbit 51226 at different heights (solid lines), with fitted spectra (dashed lines). (b) Residuals of all spectra in orbit 51226 (blue), mean of the residuals in that orbit (green) and the average ( $1\sigma$ ) thermal noise of the measurements (white).

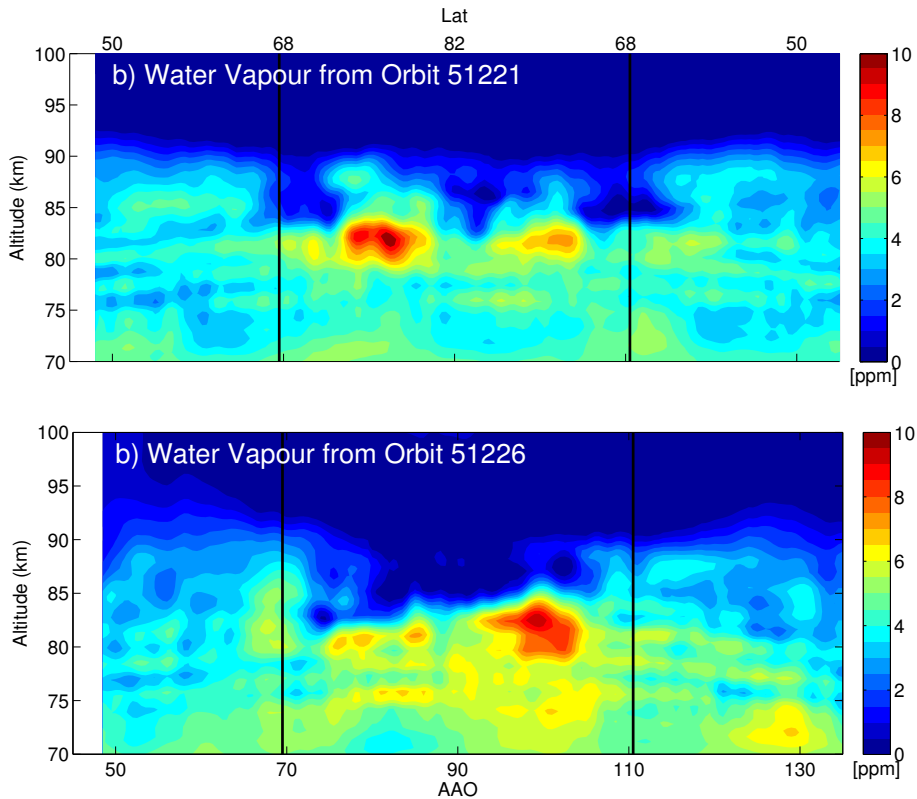


**Figure 6.** Example results from orbit 51221 and orbit 51226 on 15 July 2010. The lower x axis shows the AAO and the top axis shows the true latitude of the measurements. The black lines indicate the positions of collocated ACE-FTS and AIM-SOFIE measurements.

## Retrieval of water vapour around PMCs from Odin-SMR

O. M. Christensen et al.

Title Page	
Abstract	Introduction
Conclusions	References
Tables	Figures
◀	▶
◀	▶
Back	Close
Full Screen / Esc	
Printer-friendly Version	
Interactive Discussion	



## Retrieval of water vapour around PMCs from Odin-SMR

O. M. Christensen et al.

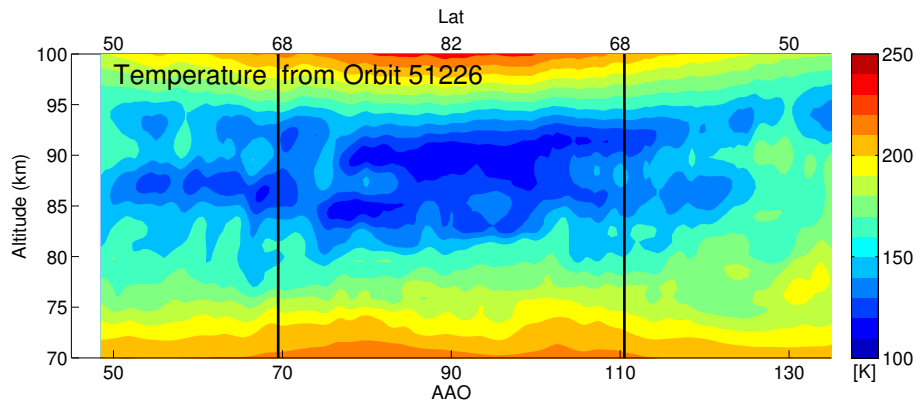


**Figure 7.** Temperature retrieved from orbit 51226 on 15 July 2010. The lower x axis shows the AAO and the top axis shows the true latitude of the measurements. The black lines indicate the positions of collocated AIM-SOFIE measurements.

[Title Page](#)[Abstract](#)[Introduction](#)[Conclusions](#)[References](#)[Tables](#)[Figures](#)[Back](#)[Close](#)[Full Screen / Esc](#)[Printer-friendly Version](#)[Interactive Discussion](#)

## Retrieval of water vapour around PMCs from Odin-SMR

O. M. Christensen et al.

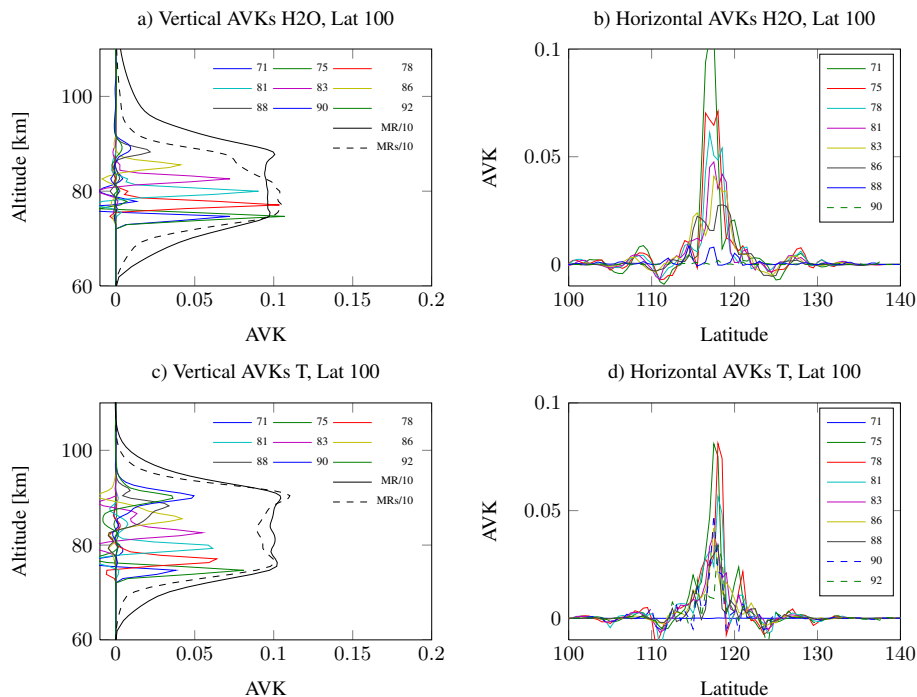


**Figure 8.** Averaging kernels for water vapour (top) and temperature (bottom), measurement response/10 for large scale differences from a priori (MR, solid), and measurement response/10 for small scale differences (MRs, dashed). The details about the two different measurement responses are explained in the text.



## Retrieval of water vapour around PMCs from Odin-SMR

O. M. Christensen et al.

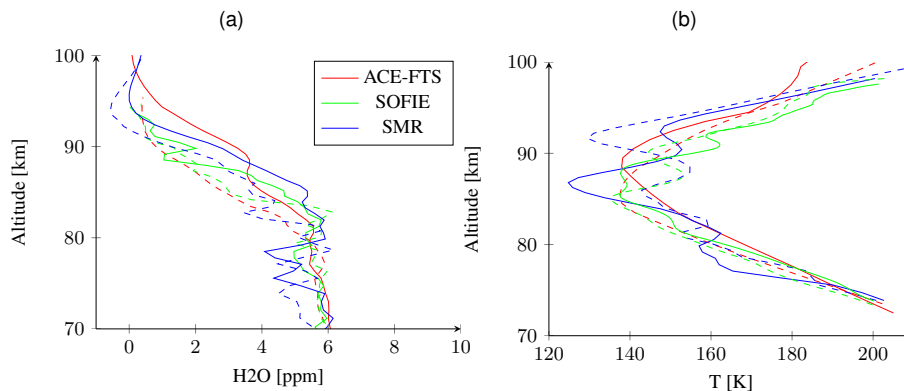


**Figure 10.** (a) Water vapour profiles from orbit 51226 at 68° N, 81° E (dashed lines) and 68° N, 63° W (solid lines) from SMR (blue), with collocated ACE-FTS (red) and SOFIE (green) measurements. (b) The corresponding temperature profiles.

[Title Page](#)[Abstract](#)[Introduction](#)[Conclusions](#)[References](#)[Tables](#)[Figures](#)[◀](#)[▶](#)[◀](#)[▶](#)[Back](#)[Close](#)[Full Screen / Esc](#)[Printer-friendly Version](#)[Interactive Discussion](#)



## Retrieval of water vapour around PMCs from Odin-SMR

O. M. Christensen et al.

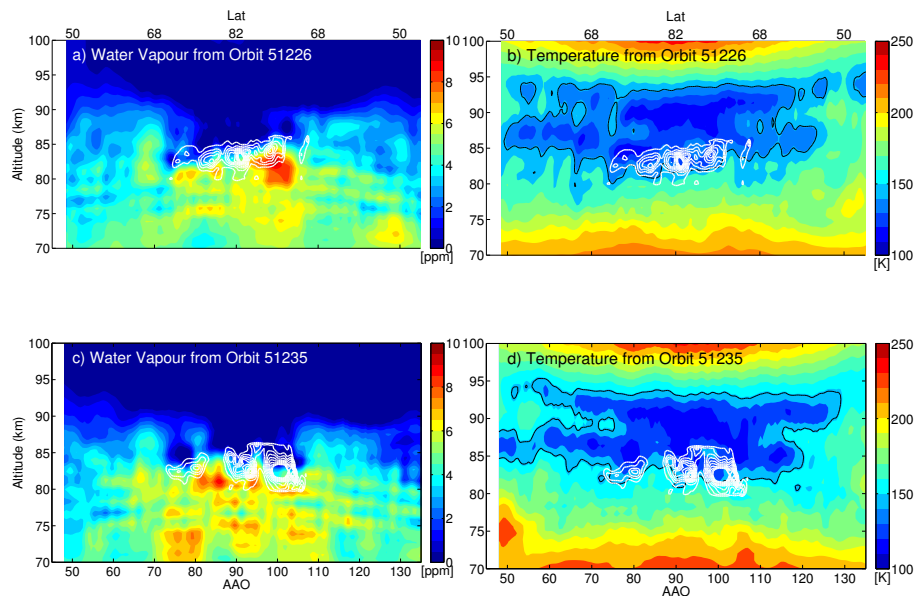


**Figure 12.** Water vapour (left column) and temperature (right column) fields from two orbits 15 July 2010. The white contours show the volume scattering coefficient from OSIRIS, where each contour corresponds to  $1 \times 10^{-9} \text{ m}^{-1} \text{ str}^{-1}$ . The 150 K temperature contour is given by the black line in the two rightmost panels. The lower  $x$  axis shows the AAO and the top axis shows the true latitude of the measurements.

Title Page

Abstract

Introduction

Conclusions

References

Tables

Figures

◀

▶

◀

▶

Back

Close

Full Screen / Esc

Printer-friendly Version

Interactive Discussion

